





Article

Inhibitors of the RBD-ACE-2 Found among a Wide Range of Dyes by the Immunoassay Method

Ekaterina D. Mordvinova ^{1,2}, Polina A. Nikitina ³ , Olga I. Yarovaya ^{1,*} , Ekaterina A. Volosnikova ², Denis E. Murashkin ² , Anastasiya A. Isaeva ², Tatiana Y. Koldaeva ³, Valery P. Perevalov ³, Nariman F. Salakhutdinov ¹ and Dmitriy N. Shcherbakov ² 

¹ Department of Medicinal Chemistry, N.N. Vorozhtsov Novosibirsk Institute of Organic Chemistry SB RAS, Lavrentyev ave., 9, 630090 Novosibirsk, Russia

² State Research Center of Virology and Biotechnology VECTOR, Rospotrebnadzor, 630559 Koltsovo, Russia

³ Department of Fine Organic Synthesis and Chemistry of Dyes, D.I. Mendeleev University of Chemical Technology of Russia, Miusskaya sq., 9, 125047 Moscow, Russia

* Correspondence: ooo@nioch.nsc.ru

Abstract: Angiotensin-converting enzyme 2 (ACE2), the functional receptor of SARS-CoV-2, plays a crucial role in the pathogenesis of COVID-19. ACE2 targeting holds the promise for preventing and inhibiting SARS-CoV-2 infection. In this work, we describe the development and use of a test system based on competitive ELISA for the primary screening of potential antiviral compounds. We studied the activity of the library of dyes of different groups. Several dyes (ortho-cresolphthalein, eosin (free acid), eosin (Na salt)) that inhibited the interaction of ACE2 with the spike proteins of SARS-CoV-2 have been identified among the candidates. A potential antiviral drug, methylene blue, did not show activity in our study. We believe that our results can help in the further search for inhibitors of interaction between the coronavirus spike protein and ACE2 receptor.

Keywords: SARS-CoV-2 virus; spike S; ELISA; RBD; dyes



Citation: Mordvinova, E.D.; Nikitina, P.A.; Yarovaya, O.I.; Volosnikova, E.A.; Murashkin, D.E.; Isaeva, A.A.; Koldaeva, T.Y.; Perevalov, V.P.; Salakhutdinov, N.F.; Shcherbakov, D.N. Inhibitors of the RBD-ACE-2 Found among a Wide Range of Dyes by the Immunoassay Method. *Chemosensors* **2023**, *11*, 135. <https://doi.org/10.3390/chemosensors11020135>

Academic Editors: Juri M. Timonen and Petri A Turhanen

Received: 25 December 2022

Revised: 2 February 2023

Accepted: 10 February 2023

Published: 13 February 2023



Copyright: © 2023 by the authors. Licensee MDPI, Basel, Switzerland. This article is an open access article distributed under the terms and conditions of the Creative Commons Attribution (CC BY) license (<https://creativecommons.org/licenses/by/4.0/>).

1. Introduction

SARS-CoV-2 is the causative agent of acute respiratory disease, referred to as COVID-19. The virus belongs to the coronavirus family (Coronaviridae), which includes the highly pathogenic MERS and SARS viruses (SARS-CoV-1) [1]. SARS-CoV-2 is an enveloped virus with a single-stranded RNA genome. Each step in the life cycle of the virus can be a potential target for drug therapy [2]. Promising targets for drugs against SARS-CoV-2 are non-structural proteins that play a role in the viral replication process such as the main viral protease 3-chymotrypsin-like protease (3CLpro), papain-like protease (PLpro), RNA-dependent RNA polymerase, or spike surface protein [3]. The surface glycoprotein S SARS-CoV-2, consisting of two subunits S1 and S2, plays an important role in viral entry by mediating receptor binding and membrane fusion [4]. The S protein binds to human angiotensin-converting enzyme 2 (ACE2), which serves as the entry receptor for the virus. Binding to ACE2 triggers another S2 subunit cleavage event, which leads to the formation of the complex required for virus–host membrane fusion [5].

Targeting the interaction between the receptor-binding domain (RBD) of the SARS-CoV-2 spike protein S and host cell ACE2 is a promising therapeutic strategy to effectively inhibit the viral entry, since binding between RBD and ACE2 is the first step in viral infection. There is currently no effective registered low molecular weight inhibitor of ACE2–S protein interaction. Significant efforts of medical chemists and virologists have focused on finding this type of inhibitor, particularly among compounds belonging to the class of dyes [6].

Testing libraries of compounds using an infectious virus allows for the search of new inhibitors of viral replication, but this requires the use of laboratories with the appropriate

level of biosafety. In this regard, surrogate models that screen potential candidates without the use of a natural virus are becoming increasingly popular. These surrogate systems can be used both directly to screen new inhibitors and to elucidate the mechanism of action of known antiviral agents. For example, to detect RBD inhibitors, a series of competitive ELISA tests have been developed to detect ligands that bind to RBD or the ACE2 cell receptor [6], an approach that has proven to be convenient for the evaluation of neutralizing antibodies [7].

In this work, we describe the development and use of a test system based on competitive ELISA to allow for the primary screening of potential antiviral agents capable of blocking the interaction of RBD with the ACE2 cell receptor. Competitive ELISA has both advantages and disadvantages. First of all, it is an inexpensive, simple, and accessible method, which can be performed by any laboratory experienced in working with recombinant proteins and ELISA. This method is amenable to automation and can therefore be implemented in a high-throughput format, allowing for rapid screening of large compound libraries in a short time frame. As the COVID-19 pandemic has shown, compound screening is one of the limiting steps in rapid drug development. An important advantage of this method is safety, as it does not require working with a live virus. The use of this method, through the use of certain proteins, makes it possible to understand the target on which the inhibitor acts. At the same time, one of the disadvantages of this method is the poor transferability of the results obtained in the *in vivo* model, as often a small number of substances selected using competitive ELISA are active in tests using a live virus. Earlier, the use of a method based on competitive ELISA allowed us to suggest the mechanism of action of entry inhibitors based on (–)-borneol [8] and derivatives of (+)-usnic acid [9]. This paper describes a study of the biological properties of different types of dyes capable of acting as SARS-CoV-2 penetration inhibitors, using both RBD and a recombinant analog of the spike protein S.

Organic dyes are relatively small molecules that are not only capable of interacting with light by absorbing and converting electromagnetic radiation energy in the visible, near-ultraviolet, and infrared regions of the spectrum, but also have an affinity to the substrates being stained. At the same time, the nature of interaction of a dye molecule with fiber macromolecules (in the case of textile dyes) or biological objects (e.g., when staining histological preparations) is determined by their structural properties. The functional groups in the structures of organic dyes enable both covalent and ionic attachment as well as hydrogen bonding, along with van der Waals and stacking interactions. The most common mechanism of dye fixation on the substrate is still the formation of ionic bonds. Despite the fact that the first synthetic organic dyes were obtained as early as the 1830s, the chemistry of organic dyes dates back to 1856, when 18-year-old William Henry Perkin, working at King's College London under A.W. von Hoffmann, obtained the diazine dye Mowin [10]. Paradoxically, this dye was obtained by accident in an attempt to synthesize quinine, a natural anti-malarial agent. What makes this story even more interesting is that just 20 years later, in 1876, Heinrich Caro at BASF produced the first fully synthetic medicine (also a dye), this time thiazine—methylene blue, which was used to treat malaria from 1891 until World War II [11,12].

Since the middle of the 19th century, a huge number of organic dyes have been produced, and not only for the textile industry. They are used in printing including the protection of valuable documents, in the food industry, in cosmetics and perfumery, in laser technology, in materials for modern electronics, in organic LEDs, as tags for biological research and for intraoperative imaging, and they are also used in photodynamic therapy. The dye molecules themselves may also have biological activity. For example, triarylmethane dyes such as brilliant green and fuchsin are widely known to have antiseptic properties. The well-known acid–base indicator phenolphthalein was used as a laxative, but was banned due to its carcinogenicity and numerous side effects. The already mentioned methylene blue has a wide spectrum of biological activity and is FDA approved for the treatment of children and adults with acquired methemoglobinemia. Methylene blue is also used to treat

blood components before transfusion. It is also known to have antiviral activity against Zika, yellow fever, Dengue, chikungunya, Ebola, and MERS viruses [13–16]. Not surprisingly, since the beginning of the COVID-19 pandemic, it has been seen as one of the antiviral candidates against SARS-CoV-2 [17–19]. It has been established that methylene blue inhibits the protein–protein interaction between the SARS-CoV-2 virus spike protein S and ACE2 of the host cell [12,20], being a non-selective inhibitor. Another known non-selective inhibitor is the xanthene dye erythrosine [21].

Organic dyes containing heterocyclic fragments of thiazine (including methylene blue), oxazine, diazine, acridine, xanthene (including erythrosine) as well as dyes and acid–base indicators of the arylmethane series (including fuchsin) were chosen as objects of research in the presented work. All of the above-mentioned dye molecules are capable of interacting with the substrate via ionic bond formation and may also participate in H-bonds, van der Waals, and hydrophobic interactions.

2. Materials and Methods

2.1. Chemistry

Synthetic organic dyes of different chemical classes were taken from the collection of organic dye samples at the Department of Technology of Fine Organic Synthesis and Chemistry of Dyes at D.I. Mendeleev University of Chemical Technology of Russia. The purity of compounds was checked before the biological tests; in all cases, the basic substance content was more than 95%.

2.2. Plasmid Construction, Recombinant Protein Expression, and Purification

The RBD and S trimer were prepared as previously described [22]. The Wuhan-1 strain spike nucleotide sequence (GenBank: MN908947) and Delta variant (B.1.617.2) (GenBank: OK529678.1) were codon-optimized and synthesized. The RBD region (308V–542N) was amplified and cloned into the pVEAL2 transposon plasmid in frame with the N-terminal spike signal sequence (MFVFLVLLPLVSSQC) and the C-terminal 10 × His-tag (pVEAL2-RBD, pVEAL2-RBDdelta). The S-protein 1M-P1213 coding gene fragment was designed with a removed protease cleavage site, K986P and V987P amino acid stabilizing substitutions, and a C-terminal T4 bacteriophage fibrin trimerization domain (GYIPEAPRDGQAYVRKDGWVLLSTFL), followed by a 10 × His-tag (pVEAL2-S, pVEAL2-Sdelta). The nucleotide sequence of chimeric human ACE2-Fc was synthesized and cloned into the pVEAL2 transposon plasmid (pVEAL2-ACE2).

For the stable expression of proteins in a Chinese hamster ovary cell line (CHO-K1), cells were transfected with the recombinant plasmids (pVEAL2-S, pVEAL2-Sdelta, pVEAL2-RBD, pVEAL2-RBDdelta, pVEAL2-ACE2), using Lipofectamine 3000 (Invitrogen, Carlsbad, CA, USA), in accordance with the manufacturer’s instructions. In order to integrate the vector expression cassette into the host genome, cells were co-transfected with the pCMV (CAT) T7-SB100 plasmid-encoding SB100 transposase. Transfected cells were selected with puromycin (10 µg/mL) for 3 days. Next, high-producing clones were isolated by dilution cloning and cultured in roller bottles at 37 °C on DMEM/F-12 medium supplemented with 2% FBS.

Recombinant proteins were isolated from the cultural medium of the CHO-K1 cells. The cultural medium was centrifuged to remove cell debris, and filtered using 0.22 µm filters. RBD and S-trimer were purified via subsequent Ni-NTA and ion-exchange chromatography as described in [23]. Recombinant ACE2-Fc was purified using a MabSelect SuRe resin (Cytiva, Uppsala, Sweden). Protein fractions were analyzed by SDS-PAGE in 15% separating polyacrylamide gel, and the target protein fraction was dialyzed against PBS. The samples of the obtained proteins were sterilized by filtration through 0.22 µm filters. The Gel-Pro Analyzer, Ver. 3.1 program determined the purity and homogeneity. The quantitative analysis of the protein content was performed by the Lowry method.

2.3. Preparation ACE2-HRP Conjugate

The purified ACE2-Fc protein was dissolved in water at a concentration of 2 mg/mL. A total of 100 mL of the 0.088 M sodium periodate solution was added to protein, then incubated in the dark for 15–20 min at room temperature. The reaction was quenched by adding glycerol. After purification, ACE2-Fc was mixed with horseradish peroxidase (HRP) at a ratio of 1:1, and incubated for 2 h at room temperature. In a fume hood, 5 M sodium cyanoborohydride was added to the reaction solution, and incubated for 30 min at room temperature with gentle mixing. The reaction was blocked by the addition of 50 μ L of 1 M ethanolamine, pH 9.6, with incubation for 30 min at room temperature. The conjugate was purified from excess reactants by dialysis, then BSA was added to 5 mg/mL glycerin. ACE2-HRP was stored at $-20\text{ }^{\circ}\text{C}$

2.4. ELISA-Based Competitive Inhibition of the RBD(S-trimer)/ACE2 Interaction

A detailed ELISA-based competitive inhibition of the RBD(S-trimer)/ACE2 interaction methodology is available in [8]. Briefly, in the wells of 96-well plates, RBD or S trimer proteins were adsorbed at a concentration of 400 ng/well in 0.01 M phosphate-buffered saline (PBS, pH 7.2), incubated for 18 h at $+4\text{ }^{\circ}\text{C}$. The plates were then washed with a PBST buffer (0.1% Tween-20 in PBS) and blocked with 1% casein in PBS-T for 1 h at $37\text{ }^{\circ}\text{C}$. Solutions of the compounds in DMSO (at a concentration of 10 mg/mL) diluted with phosphate-buffered saline to a concentration of 5 to 500 μ M were added to the wells and incubated for 1 h at $37\text{ }^{\circ}\text{C}$. To determine the specificity of the inhibitory activity, the following procedure was carried out. BSA solution (in the concentration range from 125 μ g/mL to 1 mg/mL) with the compound at the IC_{50} concentration was added to the wells and incubated for 1 h at $37\text{ }^{\circ}\text{C}$. After washing three times with PBST, recombinant ACE2 labeled with horseradish peroxidase was added at a dilution of 1/500 and incubated for 1 h at $37\text{ }^{\circ}\text{C}$. The wells were washed again and the TMB substrate solution was added. After 15 min, the reaction was stopped with 50 μ L of 1 M HCl and the absorbance was measured at 450 nm using a Varioskan Lux multi-mode microplate reader (Thermo Fisher Scientific Inc., Waltham, MA, USA). To measure the absorbance, a Varioskan Lux multi-mode microplate reader (Thermo Fisher Scientific Inc.) was used. All results shown are the average of at least two independent experiments. Inhibition was calculated by a comparison to the control wells with no inhibitor added (negative control). The IC_{50} values were determined by fitting the data with the [inhibitor] vs. normalized response models (the standard inhibition curve, GraphPad Prism).

2.5. Statistical Analysis

All statistical analyses were performed using GraphPad Prism software, San Diego, CA, USA.

3. Results and Discussion

Dyes are a large group of organic compounds capable of coloring various substances and materials. Due to their structure, dyes can bind firmly to substances via ionic, covalent, hydrogen bonding, or via adsorption forces. In medicine, dyes occupy a borderline position between antiseptic and chemotherapeutic agents. One of the disadvantages of organic dyes in therapeutic use is staining, instability in light, lack of selectivity in binding, and conformational transitions. A large number of dyes have an affinity to proteins such as common textile dyes for protein fibers (wool, silk, leather, and fur) [24].

In this work, we investigated different groups of dyes: arylamines (thiazine, oxazine, diazine), diarylmethanes, triarylmethanes, and xanthenes. Our sample of compounds included those known to be capable of non-selective inhibition such as erythrosine. Different chemical classes of dyes were investigated: arylamines (thiazines **1a,b**, **2**, **3**, oxazines **4**, **5**, and diazine dye Safranin **6**, Table 1), diarylmethane acridine dye **7** as well as several xanthene dyes (i.e., fluorescein derivatives **8–11**, and rhodamines **12**, **13**, Table 2). For methylene blue dye, two different salts **1a,b** were studied; for eosin, both the free acid **10a**

and the sodium salt **10b** were determined. The arylmethane dyes **14–28** (Table 3) and the phthalein indicators **29–34** (Table 4) were also considered. Since not all of the dyes under investigation have unambiguously recognizable trivial names, their names and color index numbers (a classifier of pigments and dyes published since 1924 by the Society of Dyers and Colorists (SDC) and the American Association of Textile Chemists and Colorists (AATCC)) are also given in Tables 1–4 for the convenient identification of compounds. Since acid–base indicators are not used in the textile industry, they were not included in this classification. We did not test the best known of the phthalein indicator dyes, phenolphthalein, because it has been banned by the FDA for medical use due to its carcinogenicity [25]. At the same time, no data on the carcinogenicity of indicators **29–34** of the same chemical class are available in the literature.

Table 1. Arylamine (phenothiazine, phenooxazine and phenodiazine) dyes.

Compound	Structure of the Compound								Name	Color Index Name (Number)	
	X	R ¹	R ²	R ³	R ⁴	R ⁵	R ⁶				
1a	S	N(CH ₃) ₂	N ⁺ (CH ₃) ₂ Cl [−]	H	H	H	H	Methylene blue (chloride)	Basic Blue 9 (52015)		
1b	S	N(CH ₃) ₂	N ⁺ (CH ₃) ₂ Cl [−]	H	H	H	H	Methylene blue (double zinc)	Basic Blue 9 (52015)		
2	S	NH ₂	N ⁺ (CH ₃) ₂ Cl [−]	CH ₃	H	H	H	Toluidine blue	Basic Blue 17 (52040)		
3	S	N(CH ₃) ₂	N ⁺ (CH ₃) ₂ Cl [−]	H	H	NO ₂	H	Methylene green	Basic Green 5 (52020)		
4	O	N(CH ₃) ₂	O	H	H	OH	COOH	Gallocyanine	Mordant Blue 10 (51030)		
5	O									Meldola's Blue	Basic Blue 6 (51175)
6	N									Safranin	Basic Red 2 (50240)

Table 2. Arylmethane heterocyclic (acridine and xanthene) dyes.

Compound	Structure						Name	Color Index Name (Number)
	X	R ¹	R ²	R ³	R ⁴	R ⁵		
7	N	H	NH ₂	NH ₂ ⁺ Cl [−]	CH ₃	H	Acridine Yellow	Basic Yellow K (46025)

Table 2. Cont.

Compound	Structure						Name	Color Index Name (Number)
	X	R ¹	R ²	R ³	R ⁴	R ⁵		
8	O		OH	O	H	H	Fluorescein	Acid Yellow 73 (45350)
9	O		OH	O	H	Br	4',5'-dibromofluorescein	Acid Orange 11 (45370)
10a	O		OH	O	Br	Br	Eosin (free acid)	Acid Red 87 (45380)
10b	O		ONa	O	Br	Br	Eosin (Na salt)	Acid Red 87 (45380)
11	O		OH	O	I	I	Erythrosine B	Solvent Red 140 (45430)
12	O		N(C ₂ H ₅) ₂	N(C ₂ H ₅) ₂ ⁺ Cl ⁻	H	H	Rhodamine B	Basic Violet 10 (45170)
13	O		N(C ₂ H ₅) ₂	N(C ₂ H ₅) ₂ ⁺ Cl ⁻	CH ₃	H	Rhodamine 6G	Basic Red 1 (45160)

Table 3. Arylmethane textile dyes.

Compound	Structure			Name	Color Index Name (Number)
	R ¹	R ²	R ₃		
14	NH ₂	CH ₃	H	Auramine O	Basic Yellow 2 (41000)
15		H	H	Fuchsin	Basic Red 9 (42500)

Table 3. Cont.

Compound	Structure	Name	Color Index Name (Number)
	<p style="text-align: center;"> R^2N R^3 R^1 R^3 NR^2Cl^- </p> <p style="text-align: center;"> R^1 R^2 R^3 </p>		
16		New Fuchsin	Basic Violet 2 (42520)
17		Crystal Violet	Basic Violet 3 (42555)
18		Methyl Green	Basic Blue 20 (42585)
19		Malachite Green	Basic Green 4 (42000)
20		Victoria Pure Blue BO	Basic Blue 7 (42595)
21		Basic Blue 3	Basic Blue 11 (44040)
22		Victoria Blue B	Basic Blue 26 (44045)
23		Permanent Purple	Basic Violet 1 (42535:2)
24		Basic Fuchsin	Basic Violet 14 (42510)

Table 3. Cont.

Compound	Structure	Name	Color Index Name (Number)
	<p style="text-align: center;"> R^1 R^2 R^3 </p>		
25		Brilliant Blue R	Acid Blue 83 (42660)
26		Chrome Azurol S	Mordant Blue 29 (43825)
27		Light Green SF	Acid Green 5 (42095)
28		Alkali Blue 4B	Acid Blue 110 (42750)

Table 4. Arylmethane phthalein indicators.

Compound	Structure				Name
	X	R ¹	R ²	R ³	
29	CO	H	CH ₃	H	o-Cresolphthalein
30	CO	CH(CH ₃) ₂	H	CH ₃	Thymolphthalein
31	CO	CH(CH ₃) ₂	CHN(CH ₂ COOH) ₂	CH ₃	Thymolphthalexone
32	SO ₂	Br	Br	H	Bromophenol Blue
33	SO ₂	CH(CH ₃) ₂	H	CH ₃	Thymol Blue
34	SO ₂	CH ₃	CHN(CH ₂ COONa) ₂	H	Xylenol Orange

Technically, the dyes in question can be classified into basic dyes **1a,b**, **2**, **3**, **5–7**, **12–24** (salts of colored organic bases), acid **8**, **9**, **10a,b**, **11**, and mordant **4**, **26** ones (salts of colored sulfonic or carboxylic acids), and acid–base indicators (compounds **29–34**).

Thus, to search for inhibitors of RBD–ACE2 interaction and test the efficacy of previously described dyes, we selected a large series of dyes belonging to different chemical classes.

3.1. The Testing System

Cell-based assays have a number of disadvantages in high-throughput compound screening. The use of cell-free assays (e.g., competitive ELISA-based variants), allows for a faster and simpler screening process. A competitive ELISA RBD/S trimer, ACE2, was chosen to test the dyes. In [6], when screening the compounds, the Fc-conjugated ACE2 receptor was the sorbed protein on the well. In our system, the sorbed protein was RBD or the full-length protein S SARS-CoV-2 (trimer), and we also used the ACE2–HRP conjugate, which allowed us to reduce the number of steps in the assay.

We used the RBD and S trimer of the Wuhan and Delta strains. Protein-dependent signal comparison showed that both full-length protein and RBD interact specifically with ACE2–HRP with a high affinity (Figure 1).

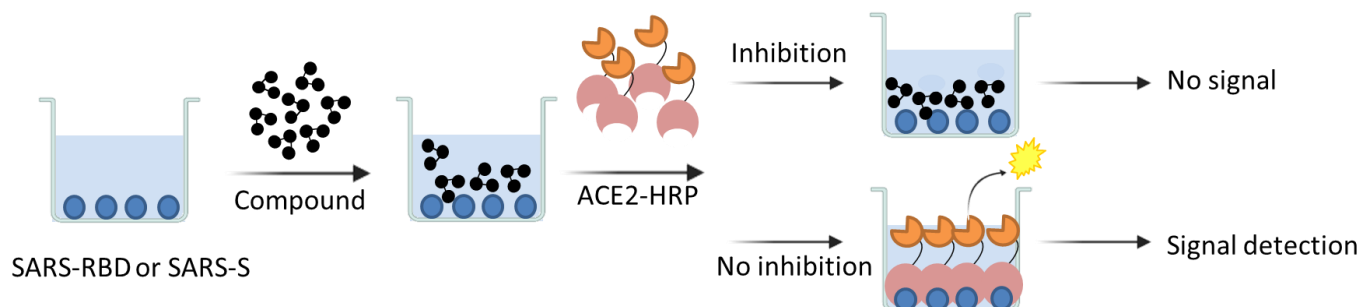


Figure 1. Scheme of a competitive ELISA. Recombinant RBD and SARS-CoV-2 protein trimer were used for sorption in the wells of the plate. After addition, incubation, and washing, recombinant ACE2–HRP was added. The substrate for HRP was then added. For the wells that inhibited the RBD–ACE2 interaction, there was no signal or it was weak. For the wells where no inhibition occurred, a signal associated with enzymatic conversion of the substrate was observed.

3.2. Screening Assays

As a first step, we explored the possibility of screening assays using a cell-free ELISA format with RBD and S trimer. We screened our library of organic dyes of different classes at 500 μM . We used the monoclonal antibody Nb6 [26] as positive controls (Figure 2).

Primary screening of the studied compounds in a single dose showed significant differences in the activity of the studied compounds, both by dye classes and by the method we used. Thus, initial testing in the RBD–ACE2 system revealed moderate activity only in the class of heterocyclic arylmethane dyes **8–13**, and the presence of the aromatic substituent R1 turned out to be extremely important—compound **7** did not show any activity at all. Compounds **26–28** related to triarylmethane derivatives showed activity. Moderate activity was also found for compounds **31** and **33**, belonging to the arylmethane phthalein indicators. The use of the trimer–RBD–ACE2 test system developed in this work expanded the range of active substances, while agents **8**, **10a**, **10b**, **11**, **27**, **29**, **30**, and **31** were still the most active.

3.3. Binding Inhibition (Concentration–Response)

For compounds **8**, **10a**, **10b**, **11**, **29**, **30**, **31**, which showed 90% inhibition at 500 μM , the semi-inhibitory concentration (IC_{50}) for the RBD and S variants of the Wuhan and Delta SARS-CoV-2 were determined (Figure 3).

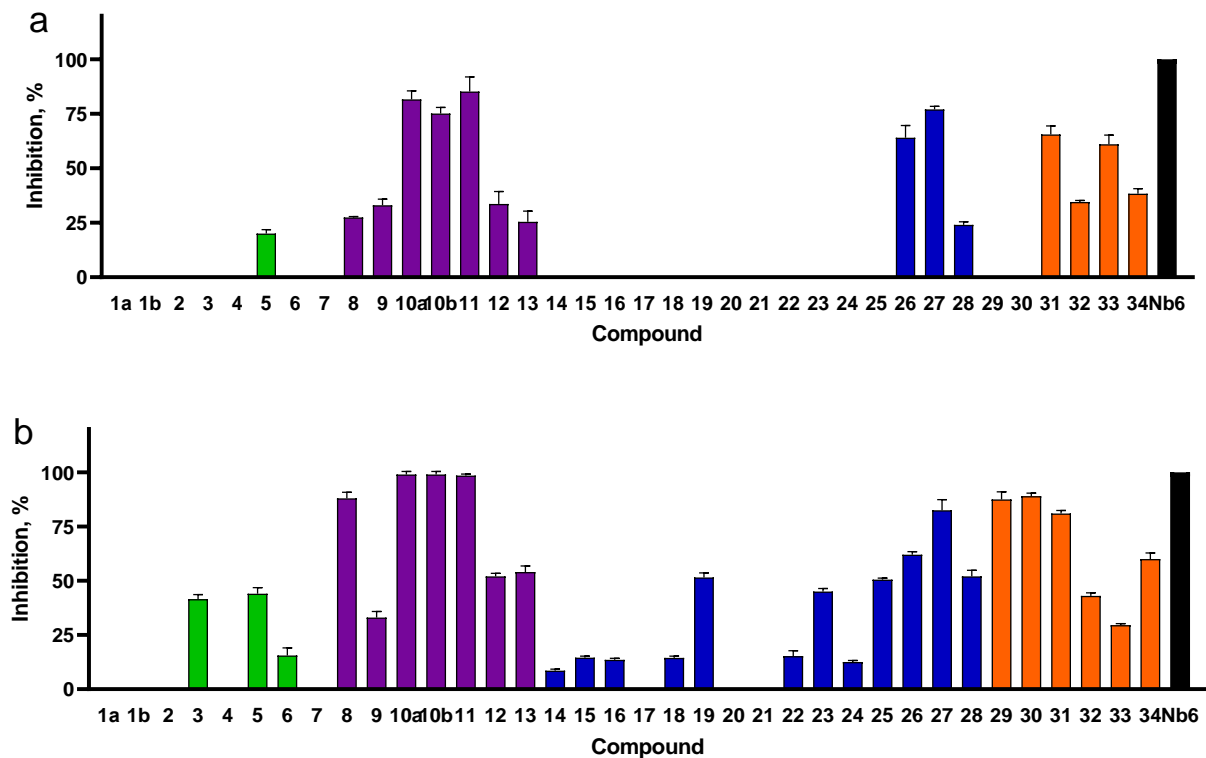


Figure 2. The inhibitory effect of compounds on SARS-CoV-2 RBD-Wuhan (a) and S trimer-Wuhan (b) binding to ACE2-HRP in our screening assay. Percent inhibition values obtained at 500 μM concentration shown normalized to the control. Erythrosine B, Nb6 were included as positive controls. The color of the columns corresponds to the following class of compounds: green—arylamine, purple—arylmethane heterocyclic, blue—arylmethane dyes, orange—phthalein.

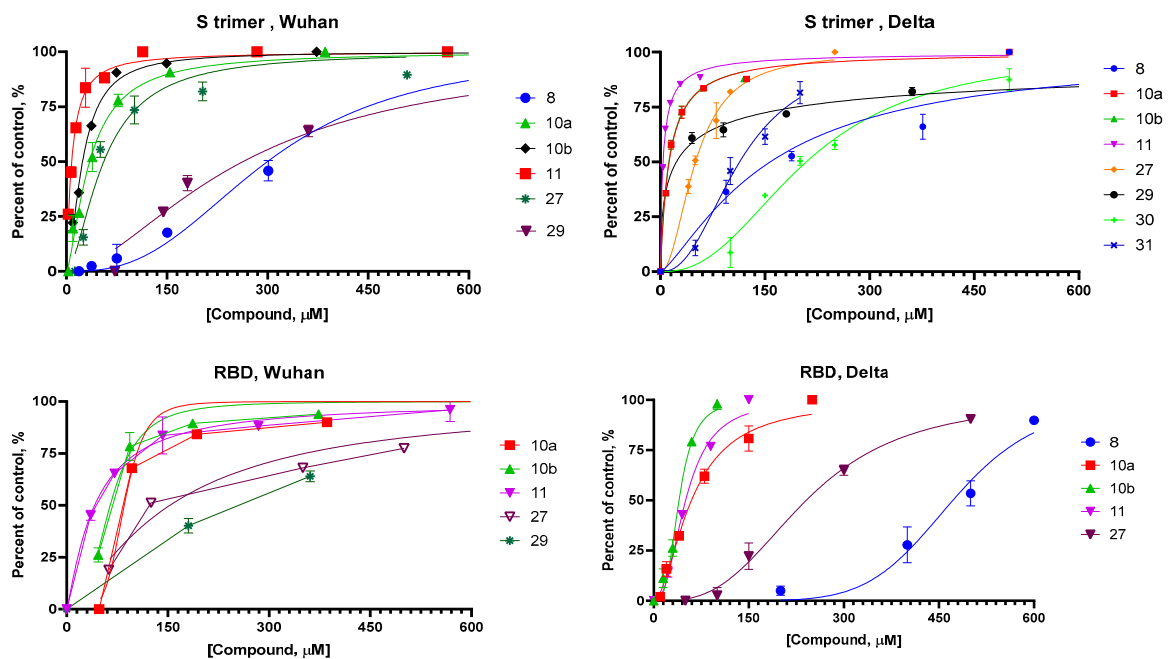


Figure 3. Concentration-dependent inhibition of SARS-CoV-2 RBD binding to ACE2 by the selected compounds. Concentration–response curves obtained in the ELISA competitive assay with RBD coated on the plate and ACE2-HRP added and the amount bound in the presence of increasing concentrations of the test compounds detected. Data (mean \pm SD for two experiments in duplicates) were normalized and fitted with standard inhibition curves; obtained IC_{50} values are shown at Table 5.

Table 5. Results of the inhibition of the SARS-CoV-2-S-RBD/S trimer binding to ACE2 compounds in the present study.

Compound	IC ₅₀ , μM RBD-Wuhan	IC ₅₀ , μM S Trimer-Wuhan	IC ₅₀ , μM RBD-Delta	IC ₅₀ , μM S Trimer-Delta
8	791 ± 9	328 ± 15	484 ± 21	168 ± 21
10a	91 ± 12	34 ± 3	66 ± 5	12 ± 5
10b	67 ± 5	24 ± 2	47 ± 6	13 ± 3
11	42 ± 1	8.5 ± 0.5	43 ± 3	3.4 ± 0.8
27	156 ± 13	58 ± 9	245 ± 8	43 ± 7
29	239 ± 14	138 ± 20	NT *	23 ± 7
30	>350	>350	NT	212 ± 24
31	>350	>350	NT	113 ± 12

* NT—not tested.

It was demonstrated that some organic dyes were able to inhibit the RBD–ACE2 interaction in a dose-dependent manner with an IC₅₀ value ranging from 40 to 800 μM (Table 5).

To avoid false-positive results, we also tested substances with the addition of a non-ionic detergent (Triton-X 100, 0.01%).

The testing of compounds in the RBD–ACE2 and S trimer–ACE2 assays showed different IC₅₀ values. This may be due to the fact that RBD, as part of the full-length S protein, has a conformation closer to the native one, while the individual RBD does not have the protein environment of the full-length protein, all of which may affect the interaction with ACE2. These features may also affect the action of inhibitors.

Methylene blue has been shown in previously published works to exhibit virulicidal activity at low micromolar concentrations in ELISA tests [6,17,20]. In our work, methylene blue 1 showed no activity, even at high concentrations above 500 μM. In the first, the reason could be the format of the assay. Our assay procedure involves sorbing the recombinant RBD or spike protein trimer, adding a potential inhibitor and incubating, and then adding the recombinant ACE2–HRP protein. This can detect substances that inhibit the interaction between RBD and ACE2–HRP by interacting with RBD. If a substance inhibits this interaction by interacting with ACE2, our analysis will not detect it. In [20], the authors showed the inhibitory activity of methylene blue in the protein interaction assay, but the assay procedure was different from the one we used. In particular, ACE2 was sorbed and RBD was added together with the substances. Second, the mechanism of the inhibitory activity of methylene blue is still unclear. A number of publications have shown that its activity requires exposure to UV [27,28]. Methylene blue possibly has an effect on another target, as part of SARS-CoV-2, that has a different RBD. Third, as shown in [29], methylene blue is very sensitive to radiation including in the visible region; as all procedures were performed in the light, perhaps during our analysis, a partial or even complete destruction of this dye occurred. In addition, situations in which some researchers identified the activity of substances and other researchers did not confirm that such activity has occurred take place quite often. For example, the authors of the paper found an activity of a natural compound 1,2,3,4,6-pentagalloylglucose (PGG) against the main viral protease 3CLpro [30], while other researchers have disproved it [31]. Therefore, the mechanism of interaction of methylene blue with SARS-CoV-2 should be studied in more detail.

To assess the specificity of the inhibitory activity of dyes for some substances, the analysis was carried out in the presence of an excess of albumin. It turned out that for substances 10a, 10b, and 11, the presence of excess albumin did not significantly affect the inhibitory activity, while for substances 27 and 31, it did. This result is not surprising, as above-mentioned, as the substances belonging to the group of dyes are often characterized by non-specific affinity to proteins [20].

Erythrosine 11 is a known random inhibitor. Compound 8 is not promiscuous in contrast to erythrosine [32]. Structurally similar to 8, ortho-cresolphthalein 29 exhibited

an activity of $IC_{50} = 23 \mu M$. The xanthene dyes **8**, **10a**, **b**, **11** turned out to be the most promising among the compounds under consideration. Switching to other heterocyclic systems had a negative effect on the manifested activity: neither acridine diarylmethane dye **7**, nor triarylamine diazine Safranin **6**, diarylamine oxazine dyes **4**, **5**, and thiazine **1a**, **b**, **2**, **3** showed any activity in our experiments. It seems that the presence of oxygen substituents in para-positions to the central carbon atom in the xanthene structure is of some importance: their replacement by nitrogen-containing ones in Rhodamines **12**, **13** resulted in a significant activity decrease.

The absence of an oxygen bridge in the structure of the molecule in the transition from xanthenes to phthaleins **29–34** also led to a decrease in the activity. Interestingly, phthalenes containing a carbonyl group in the ortho-position to the central carbon atom (**29**, **30**, **31**) were more active than those containing a sulfogroup in the same position (**32**, **33**, **34**).

The transition from hydroxytriarylmethane dyes **29–34** to triaminotriarylmethane **15–18**, **20–25**, **28** and diaminotriarylmethane derivatives **19**, **26**, **27** in most cases led to a lack of RBD inhibition (Figure 2a; except for **26**) and rather low activity with respect to S trimer inhibition (Figure 2b).

Additional substituents in the heterocyclic system of dihydroxyxanthene dyes also play a certain role. The unsubstituted fluorescein **8** was not as active as its halogen-containing analogues **9–11**. At the same time, tetrabromosubstituted eosin **10 a,b** was more active than 4',5'-dibromofluorescein **9**. It should be noted that the values of the inhibitory concentrations of the sodium salt of eosin **10a** were lower than those of free acid **10b**. The most promising activity was shown by tetraiodo substituted erythrosine **11**. It is also important to note that virtually all of the leading compounds in Table 1 are acidic dyes. Obviously, the primary interaction of the molecules under consideration with RBD originated from the formation of ionic bonds between the charged functional groups of the dye and the amino- or carbonyl group of the substrate. It may be supposed that positively charged quaternary amino groups (present in **1–3**, **5–7**, **13–24**) are less effective in binding with RBD than negatively charged sulfo- (**25–28**, **32–34**) and carbonyl- (**8–12**, **26**, **29–31**) groups. The presence of H-bond donors and acceptors in the structures of dyes provides additional fixation with the protein.

4. Conclusions

Affinity interaction systems are widely used in science and medicine. High binding constants characterizing affinity to protein–protein or protein–ligand interactions have been successfully used for the detection of viral and bacterial agents. A major advantage of these systems is their high sensitivity for the detection of small and ultra-low concentrations of the target object of interest. The interaction of the SARS-CoV-2 RBD surface protein with the ACE2 receptor is high-affinity interaction, which is required for virus penetration into target cells.

In this work, we describe the development and use of a system based on a competitive ELISA to perform the initial screening of potential antiviral agents capable of blocking the interaction of trimer S–RBD with the ACE2 cell receptor. Evaluating the obtained results, we can say that the use of trimers as a target provides greater sensitivity. More compounds showed inhibitory activity. The reason for this may be the ability of compounds to exert inhibitory activity not only through the direct inhibition of the RBD–ACE2 contact area. At the same time, the use of trimers increases the cost and complicates the procedure, since the production and purification of trimers is a more complex biotechnological task. Different types of dyes were chosen as targets for our study. Organic dyes are relatively small molecules that are not only capable of interacting with light by absorbing and converting electromagnetic radiation energy in the visible, near-ultraviolet, and infrared regions of the spectrum, but also have an affinity to the staining substrates. The functional groups in the structures of organic dyes enable both covalent and ionic bonding as well as attachment through hydrogen, van der Waals, and stacking interactions. The most common mechanism of dye attachment to the substrate being stained is still the formation of ionic bonds.

Among the compounds studied, the xanthene dyes 8, 10a,b, 11 turned out to be the most promising. Switching to other heterocyclic systems had a negative effect on the exhibited activity: neither acridium diarylmethane dye 7, nor triarylamine diazine safranin 6, nor diarylamine oxazine dyes 4, 5, and thiazine 1a,b, 2, 3 showed promising activity in our experiments. Apparently, the presence of oxygen-containing substituents in the para-position of the central carbon atom in the xanthene structure is of some importance: their substitution for nitrogen-containing ones in Rhodamine 12, 13 resulted in a considerably decreased activity. Absence of an oxygen bridge in the structure of a molecule at transition from xanthenes to phthalans 29–34 also resulted in the decrease in activity.

Author Contributions: Conceptualization, D.N.S. and O.I.Y.; Formal analysis, P.A.N. and V.P.P.; Investigation, E.D.M., E.A.V., D.E.M., A.A.I. and T.Y.K.; Methodology, O.I.Y., E.A.V. and D.N.S.; Validation, D.E.M., A.A.I. and T.Y.K.; Project administration, N.F.S. and D.N.S.; Resources, P.A.N. and V.P.P.; Visualization, E.D.M.; Supervision, V.P.P. and N.F.S.; Writing—original draft, E.D.M., P.A.N. and O.I.Y.; Writing—review & editing, P.A.N., O.I.Y., N.F.S. and D.N.S. All authors have read and agreed to the published version of the manuscript.

Funding: The purity of the substances tested was confirmed with the support of the Ministry of Science and Higher Education of the Russian Federation (No. 1021051703312-0-1.4.1). Method development and biological testing was supported by the Ministry of Science and Higher Education of the Russian Federation (Agreement No. 075-15-2021-1355 dated 12 October 2021) as part of the implementation of certain activities of the Federal Scientific and Technical Program for the Development of Synchrotron and Neutron Research and Research Infrastructure for 2019–2027.

Institutional Review Board Statement: Not applicable.

Informed Consent Statement: Not applicable.

Data Availability Statement: Not applicable.

Conflicts of Interest: The authors declare no conflict of interest.

References

1. Novikov, F.N.; Stroylov, V.S.; Svitanko, I.V.; Nebolsin, V.E. Molecular basis of COVID-19 pathogenesis. *Russ. Chem. Rev.* **2020**, *89*, 858–878. [[CrossRef](#)]
2. Yan, W.; Zheng, Y.; Zeng, X.; He, B.; Cheng, W. Structural biology of SARS-CoV-2: Open the door for novel therapies. *Signal Transduct. Target. Ther.* **2022**, *7*, 26. [[CrossRef](#)]
3. Ghosh, A.K.; Mishevich, J.L.; Mesecar, A.; Mitsuya, H. Recent Drug Development and Medicinal Chemistry Approaches for the Treatment of SARS-CoV-2 Infection and COVID-19. *ChemMedChem* **2022**, *17*, e202200440. [[CrossRef](#)]
4. Tang, T.; Bidon, M.; Jaimes, J.A.; Whittaker, G.R.; Daniel, S. Coronavirus membrane fusion mechanism offers a potential target for antiviral development. *Antivir. Res.* **2020**, *178*, 104792. [[CrossRef](#)]
5. Walls, A.C.; Park, Y.-J.; Tortorici, M.A.; Wall, A.; McGuire, A.T.; Velesler, D. Structure, Function, and Antigenicity of the SARS-CoV-2 Spike Glycoprotein. *Cell* **2020**, *181*, 281–292. [[CrossRef](#)]
6. Bojadzic, D.; Alcazar, O.; Chen, J.; Chuang, S.-T.; Condor Capcha, J.M.; Shehadeh, L.A.; Buchwald, P. Small-Molecule Inhibitors of the Coronavirus Spike: ACE2 Protein–Protein Interaction as Blockers of Viral Attachment and Entry for SARS-CoV-2. *ACS Infect. Dis.* **2021**, *7*, 1519–1534. [[CrossRef](#)]
7. Limonta-Fernández, M.; China-Santiago, G.; Martín-Dunn, A.M.; Gonzalez-Roche, D.; Bequet-Romero, M.; Marquez-Perera, G.; González-Moya, I.; Canaan-Haden-Ayala, C.; Cabrales-Rico, A.; Espinosa-Rodríguez, L.A.; et al. An engineered SARS-CoV-2 receptor-binding domain produced in *Pichia pastoris* as a candidate vaccine antigen. *New Biotechnol.* **2022**, *72*, 11–21. [[CrossRef](#)]
8. Yarovaya, O.I.; Shcherbakov, D.N.; Borisevich, S.S.; Sokolova, A.S.; Gureev, M.A.; Khamitov, E.M.; Rudometova, N.B.; Zybina, A.V.; Mordvinova, E.D.; Zaykovskaya, A.V.; et al. Borneol Ester Derivatives as Entry Inhibitors of a Wide Spectrum of SARS-CoV-2 Viruses. *Viruses* **2022**, *14*, 1295. [[CrossRef](#)]
9. Filimonov, A.S.; Yarovaya, O.I.; Zaykovskaya, A.V.; Rudometova, N.B.; Shcherbakov, D.N.; Chirkova, V.Y.; Baev, D.S.; Borisevich, S.S.; Luzina, O.A.; Pyankov, O.V.; et al. (+)-Usnic Acid and Its Derivatives as Inhibitors of a Wide Spectrum of SARS-CoV-2 Viruses. *Viruses* **2022**, *14*, 2154. [[CrossRef](#)]
10. Holme, I. Sir William Henry Perkin: A review of his life, work and legacy. *Color. Technol.* **2006**, *122*, 235–251. [[CrossRef](#)]
11. Shi, G.; Shen, Q.; Zhang, C.; Ma, J.; Mohammed, A.; Zhao, H. Efficacy and Safety of Gabapentin in the Treatment of Chronic Cough: A Systematic Review. *Tuberc. Respir. Dis.* **2018**, *81*, 167. [[CrossRef](#)] [[PubMed](#)]

12. Chuang, S.-T.; Papp, H.; Kuczmog, A.; Eells, R.; Condor Capcha, J.M.; Shehadeh, L.A.; Jakab, F.; Buchwald, P. Methylene Blue Is a Nonspecific Protein–Protein Interaction Inhibitor with Potential for Repurposing as an Antiviral for COVID-19. *Pharmaceuticals* **2022**, *15*, 621. [[CrossRef](#)] [[PubMed](#)]
13. Fryk, J.J.; Marks, D.C.; Hobson-Peters, J.; Prow, N.A.; Watterson, D.; Hall, R.A.; Young, P.R.; Reichenberg, S.; Sumian, C.; Faddy, H.M. Dengue and chikungunya viruses in plasma are effectively inactivated after treatment with methylene blue and visible light. *Transfusion* **2016**, *56*, 2278–2285. [[CrossRef](#)] [[PubMed](#)]
14. Eickmann, M.; Gravemann, U.; Handke, W.; Tolksdorf, F.; Reichenberg, S.; Müller, T.H.; Seltsam, A. Inactivation of Ebola virus and Middle East respiratory syndrome coronavirus in platelet concentrates and plasma by ultraviolet C light and methylene blue plus visible light, respectively. *Transfusion* **2018**, *58*, 2202–2207. [[CrossRef](#)]
15. Faddy, H.M.; Fryk, J.J.; Hall, R.A.; Young, P.R.; Reichenberg, S.; Tolksdorf, F.; Sumian, C.; Gravemann, U.; Seltsam, A.; Marks, D.C. Inactivation of yellow fever virus in plasma after treatment with methylene blue and visible light and in platelet concentrates following treatment with ultraviolet C light. *Transfusion* **2019**, *59*, 2223–2227. [[CrossRef](#)]
16. Wang, Y.; Ren, K.; Liao, X.; Luo, G.; Kumthip, K.; Leetrakool, N.; Li, S.; Chen, L.; Yang, C.; Chen, Y. Inactivation of Zika virus in plasma and derivatives by four different methods. *J. Med. Virol.* **2019**, *91*, 2059–2065. [[CrossRef](#)]
17. Ghahestani, S.M.; Shahab, E.; Karimi, S.; Madani, M.H. Methylene blue may have a role in the treatment of COVID-19. *Med. Hypotheses* **2020**, *144*, 110163. [[CrossRef](#)]
18. Gendrot, M.; Andreani, J.; Duflo, L.; Boxberger, M.; Le Bideau, M.; Mosnier, J.; Jardot, P.; Fonta, I.; Rolland, C.; Bogreau, H.; et al. Methylene blue inhibits replication of SARS-CoV-2 in vitro. *Int. J. Antimicrob. Agents* **2020**, *56*, 106202. [[CrossRef](#)]
19. Scigliano, G.; Scigliano, G.A. Methylene blue in covid-19. *Med. Hypotheses* **2021**, *146*, 110455. [[CrossRef](#)]
20. Bojadzic, D.; Alcazar, O.; Buchwald, P. Methylene Blue Inhibits the SARS-CoV-2 Spike–ACE2 Protein-Protein Interaction—a Mechanism that can Contribute to its Antiviral Activity against COVID-19. *Front. Pharmacol.* **2021**, *11*, 2255. [[CrossRef](#)]
21. Li, Z.; Xu, J.; Lang, Y.; Wu, X.; Hu, S.; Samrat, S.K.; Tharappel, A.M.; Kuo, L.; Butler, D.; Song, Y.; et al. In vitro and in vivo characterization of erythrosin B and derivatives against Zika virus. *Acta Pharm. Sin. B* **2022**, *12*, 1662–1670. [[CrossRef](#)] [[PubMed](#)]
22. Merkuleva, I.A.; Shcherbakov, D.N.; Borgoyakova, M.B.; Shanshin, D.V.; Rudometov, A.P.; Karpenko, L.I.; Belenkaya, S.V.; Isaeva, A.A.; Nesmeyanova, V.S.; Kazachinskaja, E.I.; et al. Comparative Immunogenicity of the Recombinant Receptor-Binding Domain of Protein S SARS-CoV-2 Obtained in Prokaryotic and Mammalian Expression Systems. *Vaccines* **2022**, *10*, 96. [[CrossRef](#)] [[PubMed](#)]
23. Merkuleva, I.A.; Shcherbakov, D.N.; Borgoyakova, M.B.; Isaeva, A.A.; Nesmeyanova, V.S.; Volkova, N.V.; Aripov, V.S.; Shanshin, D.V.; Karpenko, L.I.; Belenkaya, S.V.; et al. Are Hamsters a Suitable Model for Evaluating the Immunogenicity of RBD-Based Anti-COVID-19 Subunit Vaccines? *Viruses* **2022**, *14*, 1060. [[CrossRef](#)] [[PubMed](#)]
24. Yaneva, Z.; Ivanova, D.; Nikolova, N.; Toneva, M. Organic dyes in contemporary medicinal chemistry and biomedicine. I. From the chromophore to the bioimaging/bioassay agent. *Biotechnol. Biotechnol. Equip.* **2022**, *36*, 1–14. [[CrossRef](#)]
25. Saeidnia, S.; Manayi, A. Phenolphthalein. In *Encyclopedia of Toxicology*; Elsevier: Amsterdam, The Netherlands, 2014; Volume 3, pp. 877–880. ISBN 9780123864543.
26. Schoof, M.; Faust, B.; Saunders, R.A.; Sangwan, S.; Rezelj, V.; Hoppe, N.; Boone, M.; Billesbølle, C.B.; Puchades, C.; Azumaya, C.M.; et al. An ultrapotent synthetic nanobody neutralizes SARS-CoV-2 by stabilizing inactive Spike. *Science* **2020**, *370*, 1473–1479. [[CrossRef](#)]
27. Svyatchenko, V.A.; Nikonov, S.D.; Mayorov, A.P.; Gelfond, M.L.; Loktev, V.B. Antiviral photodynamic therapy: Inactivation and inhibition of SARS-CoV-2 in vitro using methylene blue and Radachlorin. *Photodiagnosis Photodyn. Ther.* **2021**, *33*, 102112. [[CrossRef](#)]
28. Lobo, C.S.; Rodrigues-Santos, P.; Pereira, D.; Núñez, J.; Trêpa, J.C.D.; Sousa, D.L.; Lourenço, J.V.; Coelho, M.F.; de Almeida, L.P.; da Cunha, J.S.; et al. Photodynamic disinfection of SARS-CoV-2 clinical samples using a methylene blue formulation. *Photochem. Photobiol. Sci.* **2022**, *21*, 1101–1109. [[CrossRef](#)]
29. Chen, P.; Liang, Y.; Xu, Y.; Zhao, Y.; Song, S. Synchronous photosensitized degradation of methyl orange and methylene blue in water by visible-light irradiation. *J. Mol. Liq.* **2021**, *334*, 116159. [[CrossRef](#)]
30. Chiou, W.-C.; Chen, J.-C.; Chen, Y.-T.; Yang, J.-M.; Hwang, L.-H.; Lyu, Y.-S.; Yang, H.-Y.; Huang, C. The inhibitory effects of PGG and EGCG against the SARS-CoV-2 3C-like protease. *Biochem. Biophys. Res. Commun.* **2022**, *591*, 130–136. [[CrossRef](#)]
31. Tan, H.; Ma, C.; Wang, J. Invalidation of dieckol and 1,2,3,4,6-pentagalloylglucose (PGG) as SARS-CoV-2 main protease inhibitors and the discovery of PGG as a papain-like protease inhibitor. *Med. Chem. Res.* **2022**, *31*, 1147–1153. [[CrossRef](#)]
32. Ganesan, L.; Margolles-Clark, E.; Song, Y.; Buchwald, P. The food colorant erythrosine is a promiscuous protein-protein interaction inhibitor. *Biochem. Pharmacol.* **2011**, *81*, 810–818. [[CrossRef](#)] [[PubMed](#)]

Disclaimer/Publisher’s Note: The statements, opinions and data contained in all publications are solely those of the individual author(s) and contributor(s) and not of MDPI and/or the editor(s). MDPI and/or the editor(s) disclaim responsibility for any injury to people or property resulting from any ideas, methods, instructions or products referred to in the content.